Imperial College London

The Hamlyn Centre for Robotic Surgery

Toward a Versatile Robotic Platform for Fluoroscopy and MRI-Guided Endovascular Interventions: A Pre-Clinical Study

Mohamed E. M. K. Abdelaziz, Dennis Kundrat, Marco Pupillo, Giulio Dagnino, Trevor M. Y. Kwok, Wenqiang Chi, Vincent Groenhuis, Françoise J. Siepel, Celia Riga, Stefano Stramigioli, Guang-Zhong Yang

Submitted: March 1, 2019. Accepted: June 20, 2019

To be published in:

2019 IEEE/RSJ International Conference on Intelligent Robots and Systems (IROS)

To cite this paper:

M. E. M. K. Abdelaziz, D. Kundrat, M. Pupillo, G. Dagnino, T. M. Y. Kwok, W. Chi, V. Groenhuis, F. J. Siepel, C. Riga, S. Stramigioli, G.Z. Yang, “Toward a Versatile Robotic Platform for Fluoroscopy and MRI-Guided Endovascular Interventions: A Pre-Clinical Study”, in *2019 IEEE/RSJ International Conference on Intelligent Robots and Systems (IROS),* 2019.

Toward a Versatile Robotic Platform for Fluoroscopy and MRI-Guided Endovascular Interventions: A Pre-Clinical Study

Mohamed E. M. K. Abdelaziz[1], Dennis Kundrat[1], Marco Pupillo[1], Giulio Dagnino[1], Trevor M. Y. Kwok[2], Wenqiang Chi[1], Vincent Groenhuis[3], Françoise J. Siepel[3], Celia Riga[2], Stefano Stramigioli[3], Guang-Zhong Yang[1,4]

***Abstract*— Cardiovascular diseases remain as the most common cause of death worldwide. Remotely manipulated robotic systems are utilized to perform minimally invasive endovascular interventions. The main benefits of this methodology include reduced recovery time, improvement of clinical skills and procedural facilitation. Currently, robotic assistance, precision, and stability of instrument manipulation are compensated by the lack of haptic feedback and an excessive amount of radiation to the patient. This paper proposes a novel master-slave robotic platform that aims to bring the haptic feedback benefit on the master side, providing an intuitive user interface, and clinical familiar workflow. The slave robot is capable of manipulating conventional catheters and guidewires in multi-modal imaging environments. The system has been initially tested in a phantom cannulation study under fluoroscopic guidance, evaluating its reliability and procedural protocol. As the slave robot has been entirely produced by additive manufacturing and using pneumatic actuation, MR compatibility is enabled and was evaluated in a preliminary study. Results of both studies strongly support the applicability of the robot in different imaging environments and prospective clinical translation.**

I. INTRODUCTION

Cardiovascular diseases (CVDs) are a global health threat accounting for one third of all deaths (17.9 million each year) worldwide [1]. CVDs are disorders and diseases affecting the heart or blood vessels, which lead to heart attacks and strokes. However, with the combined efforts of surgeons, radiologists, cardiologists, physicists and engineers, endovascular interventions have become a mainstay of treatment for vascular diseases. These minimally invasive and image-guided treatments are performed by manipulating thin and flexible instruments (catheters and guidewires) to targeted blood vessels combined with different treatment options including stenting, embolization and ablation. These procedures not only reduce the recovery time of patients, they also decrease operating time, hospitalization, and overall time to recovery. Recently, there has been a growing interest in robotic platforms that can perform the tasks mentioned above. Compared to manual interventions, these systems can improve precision, stability, and comfort, eliminating physiological tremor and reducing radiation exposure both for patients and operators.

Research supported by the UK EPSRC (EP/N024877/1). [1]M. E. M. K. Abdelaziz, D. Kundrat, M. Pupillo, G. Dagnino, W. Chi, G. Z. Yang are with The Hamlyn Centre for Robotic Surgery, Imperial College London, UK. (e-mail: m.abdelaziz16@imperial.ac.uk). [2]T. M. Y. Kwok and C. Riga are with the Faculty of Medicine, Department of Surgery and Cancer, Imperial College London, UK. [3]V. Groenhuis, F. J. Siepel and S. Stramigioli are with Robotics and Mechatronics, University of Twente, Enschede, Netherlands.[4] G. Z. Yang is also affiliated with the Institute of Medical Robotics, Shanghai Jiao Tong University, China.

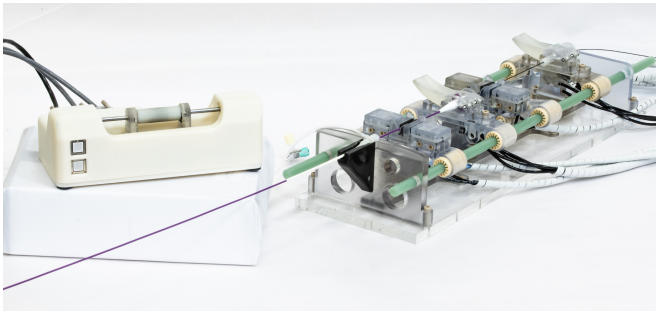

Fig. 1: Novel robotic platform with versatile, MR-safe slave robot (right) and intuitive master device (left) for endovascular interventions.

A. State of the Art

A variety of robotic systems for endovascular or cardiac catheterization were reported in research or translated to commercialisation. In general, such systems show low levels of robotic autonomy [2] and consider a master-slave set-up for teleoperated manipulation of instrumentation. Commercial systems targeting different fields of application in endovascular and cardiac cases comprise the *Magellan* and *Sensei*® X2 platforms (AurisHealth, Redwood city, CA, USA), the *Amigo* platform (Catheter Precision, Mt. Olive, NJ, USA), the *R-one*™ robot (Robocath, Rouen, France), or the *CorPath*® *GRX* platform (Corindus, Waltham, MA, USA). The corresponding master, with human machine interfaces (HMI), make use of conventional stationary joysticks, hand-held joysticks, or 3D input devices with force feedback capabilities. Commercial platforms enable electromechanical manipulation of customised (steerable) catheters and guidewires in up to 6 degrees of freedom (DOF) and were successfully used in clinical scenarios [3]–[6]. Novel master devices were proposed to improve the transparency of teleoperation. Exemplary, motion due to manipulation of standard catheters was sensed without user feedback and replicated to a slave robot [7]. More recently, magnetorheological fluid was used in combination with a catheter to mimic friction and generate user feedback [8]. Slave robots generally show alternative concepts with different electromechanical mechanisms for driving and clamping of instrumentation as reported in [9]–[11]. Device compliance with MR environments is restricted to [12], [13] and focuses on steerable catheters. For the sake of completeness, the reader is kindly referred to a comprehensive review of devices [14].

B. Limitations & Contribution

Related work has highlighted a range of emerging catheterisation platforms for endovascular or cardiac applications.

However, devices show a number of limitations regarding clinical translation: (1) Use of different standard catheters and guidewires with reported devices is limited and generally requires manufacturer-specific instruments. This impedes a cost-effective and versatile application. (2) Usability of the teleoperation set-up neglects established manual procedures. HMIs rarely imitate the human motion patterns of the procedure, e.g. joysticks. Also, many systems lack force feedback, or, when present, it is provided through commercial interfaces or joysticks, not properly capturing surgeons' skills. (3) Collaborative instrument handling, i.e. quick and easy transition between manual and robotic manipulation is currently disregarded. Robotic assistance is predominantly required for challenging cannulation tasks or instrument deployment. (4) Fluoroscopy is still considered the gold standard for robotic assistance. X-ray exposure is only reduced for the user. This limits use to pediatric patients. (5) Future directions are towards MRI-based interventions to reduce ionizing radiation exposure [15], [16]. MR-compatible devices are exclusively reported for cardiac cases with steerable catheters.

In order to overcome the aforementioned limitations, this work proposes the design and preliminary evaluation of a versatile robotic master-slave platform and navigation framework for manipulation of standard endovascular instruments in multi-modal imaging environments, e.g. fluoroscopy and MRI. Inspired by previous work [17], [18], a novel master manipulator is introduced as HMI. The device imitates the human motion pattern of translating and rotating instruments during catherisation. Furthermore, the user can perceive haptic and visual feedback related to the device or procedural states. The design of the slave robot, in particular addresses the aspect of versatility from two directions: 1.) The robotic instrument interface enables intuitive use and fast exchange of standard endovascular instruments (catheters, guidewires) to extend the range of potential clinical applications. 2.) Take advantage of additive manufacturing and pneumatic actuation to establish full compliance of the slave robot with MR safety guidelines facilitating robotic assistance in different imaging environments. This in particular targets clinical cases of pediatric MRI-guided catheterization, as exposure to x-rays is not recommended or possible. The proposed platform is evaluated in combination with a navigation framework in a study on manual and robotic vessel cannulation under fluoroscopy and an MRI-compatibility test. Results strongly motivate versatile robotic platforms that take emerging trends in medical imaging into account and improve outcomes for patients and clinical users.

II. Clinical Requirements

Clinical requirements were established by reviewing prior art (e.g. [7], [19]), analysing various endovascular procedures and interviewing vascular surgeons. Such specifications can be summarised as follows. The system should be versatile and capable to perform different vascular interventions (i.e. lower limb peripheral, aortic, iliac, carotid, visceral, upper limb peripheral, cardiac and coronary interventions). This requires the system to accommodate a wide selection of instruments (i.e. catheters and guidewires) available on the market [20] and precisely manipulate them. The system should include a navigation system to visualize the surgical site and provide image and haptic guidance to minimise contacts between the manipulated instrument and the endothelial wall. The system should be compatible with different imaging modalities, including x-ray fluoroscopy and MRI. The system should be teleoperated to remove or minimize the exposure of surgeons to x-rays. The surgeon should be always in control of the procedure and his/her motion skills should be captured by the system and properly translated to the surgical site. The system should be hands-on, easy-to-use and have a small footprint to be well integrated within the clinical workflow. In terms of safety, the procedure should be quickly revertible to manual, and the surgeon should be able to take over in a few seconds. Thus, the system should have a quick and simple method to dock and release catheters and guidewires. Finally, the system should not be harmful for both patient and operators.

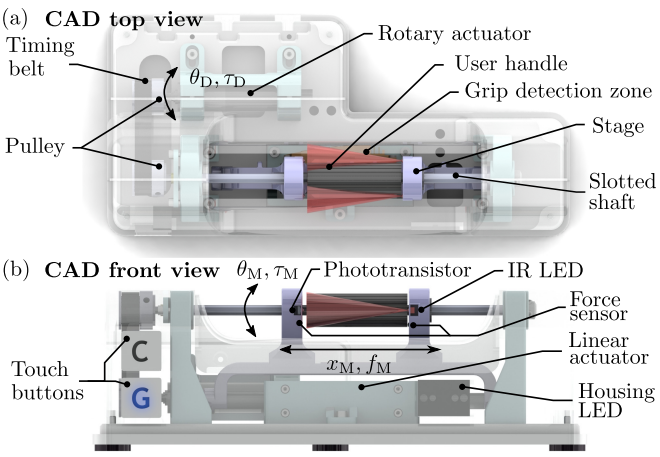

Fig. 2: Conceptual design and prototype of the proposed haptic master with electro-mechanical set-up and sensing: (a) Top and (b) front view of the CAD model.

III. Robotic Design

The design of the robotic platform addresses the clinical requirements reported above. This section describes the master and slave, while the next section reports their integration with the navigation system and the control architecture. The reader is kindly referred to the supplemental video for details on the robotic design and presentation of motion sequences.

A. Haptic Master Device

The concept of the proposed haptic master for teleoperated intervention was initially reported in [18] and fundamentally revised in this contribution with regard to mechanical design, usability, and user interaction. Design objectives of the device, presented in Fig. 2, target to mimic and map the established manual intra-procedural handling of standard catheters and guidewires to the master device for improved teleoperation transparency and intuitive user assistance. Hence, a cylindrical user handle attached to a robotic stage represents the core component of the HMI and imitates

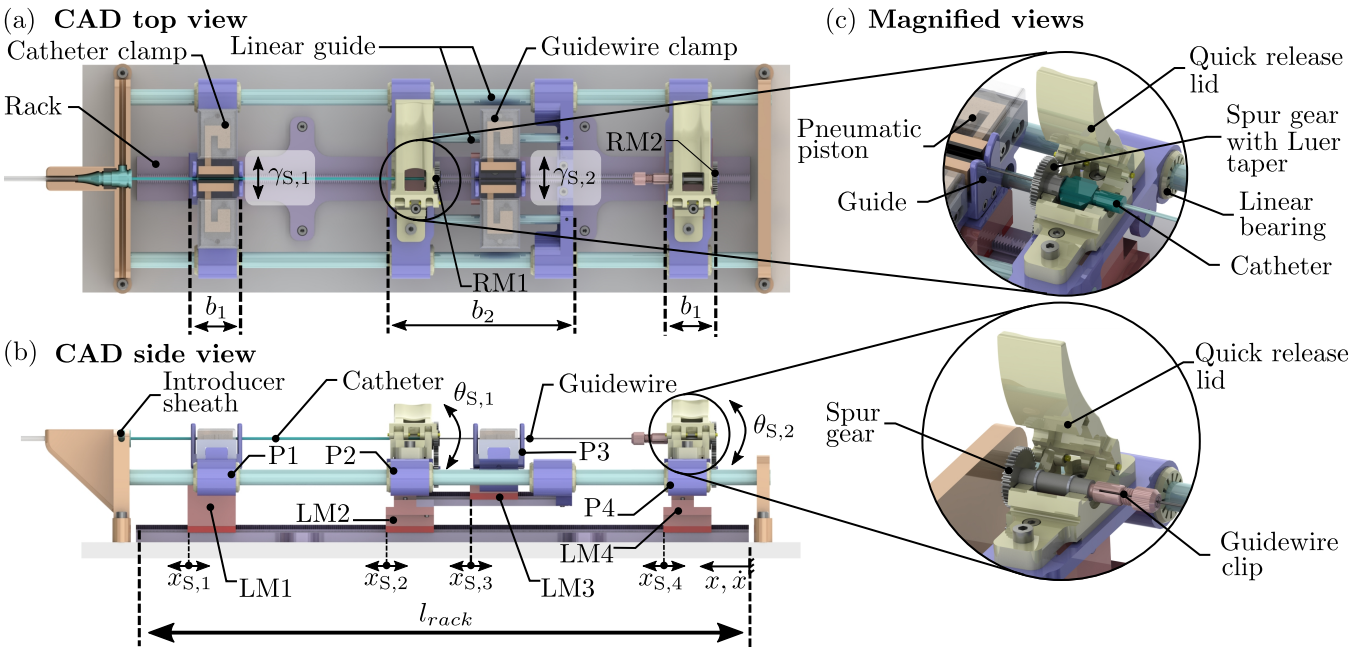

Fig. 3: Conceptual design of the proposed slave robot: (a) Top and (b) side view of the CAD model, and (c) magnified details of quick release instrumentation mounting and mechanism for introduction of rotary motion to catheter and guidewire.

the clinically established interaction and executable DOF of standard catheters and guidewires. More precisely, the handle mounts a torque-resistant linear bushing that slides on a slotted shaft (custom-made component, Bosch Rexroth GmbH, Lohr am Main, Germany). This enables the user to grip the handle and introduce displacement x_M along the shaft axis. Simultaneously, the mechanical design of the bushing allows for angular displacement θ_M of the shaft. Thus, two DOF can be executed, i.e. feeding/retraction and rotation. Haptic feedback is generated in corresponding DOF with a linear and a rotary BLDC motor (1247 and 1226 B012, Faulhaber GmbH, Schönaich, Germany) that use appurtenant motion controllers with CAN interface (MCLM/MCBL 3006, Faulhaber GmbH, Schönaich, Germany). The customised shaft enables stationary mounting of both motors and improved dynamics due to reduced moving mass and less space incorporation. In detail, torques perceived by the user yield to $\tau_\mathrm{M} = i_\mathrm{G} i_\mathrm{P} \tau_\mathrm{D}$ with gear transmission $i_\mathrm{G} = 16$, pulley transmission $i_\mathrm{P} = 1$, and drive-sided torque τ_D. Forces of the linear actuator along the shaft axis are described by f_M with maximum stroke lengths of $\pm 20\,\mathrm{mm}$. Disturbances due to mechanical friction are neglected. After user displacement, the linear motor homes the stage back to the initial (central) position, providing the user with sufficient stroke to carry on with the linear manipulation. The master joint state is described by

$$\boldsymbol{q}_\mathrm{M} = \left(x_\mathrm{M}, \theta_\mathrm{M}, \dot{x}_\mathrm{M}, \dot{\theta}_\mathrm{M}, f_\mathrm{M}, \tau_\mathrm{M}\right)^\mathrm{T} \in \mathbb{R}^6. \tag{1}$$

Complementary to the electro-mechanical design of the HMI, the contribution proposes an integration of safe, reliable, and robust user interaction. Thus, user actions are continuously monitored during manipulation. The user intention related to the direction of linear motion x_M is detected with uniaxial force sensors (FSS1500NSB, Honeywell International Inc., Charlotte, NC, USA). The latter measure interaction forces in between handle and stage. Acquired voltages are processed with a moving average filter of window size of $N = 10$. If threshold σ_F is exceeded on one of the sensors, the intended direction is set in accordance with the sensor location. Additionally, contactless detection of handle interaction is implemented with two pairs of subminiature IR LEDs (VSMY2850G, Vishay, Malvern, PA, USA) and phototransistors (SFH 3015, Osram AG, Munich, Germany). Sensor pairs are mounted in parallel to the cylindrical handle to detect user contacts in the area covered by red cones shown in Fig. 2. Lastly, visual feedback is provided for indication of system conditions (idle, ready, error) and generated by modulation (sweeping, continuous, or flashing) of housing illumination. Likewise, capacitive illuminated touch buttons at the front of the device enable an intuitive selection of the desired slave mode, i.e. manipulation of catheter or guidewire. The overall dimensions of the current prototype are $(190 \times 90 \times 64)\,\mathrm{mm}^3$.

B. Slave Robot

1) Robot Design

To address the clinical and technical requirements presented in Sec. II, a versatile pneumatically actuated robot with 4-DOF was developed to manipulate off-the-shelf angiographic catheters and guidewires by emulating the haptic master device. Each instrument is driven by two pneumatic linear stepper motors to translate the instrument, one pneumatic rotational stepper motor to rotate the instrument, and two pneumatic J-clamps to clamp while translating the instrument. The robot base measures $(500 \times 140 \times 100)\,\mathrm{mm}^3$. The conceptual design of the slave robot is shown in Fig. 3 and comprises the following platforms:

- Catheter Feeding Platform (P1): Linear stepper motor

(LM1) carrying two J-clamps,
- Catheter Following/Rotation Platform (P2): Linear stepper motor (LM2) carrying a rotary stepper motor (RM1), a catheter hub docking station, and a guidewire feeding platform (P3),
- Guidewire Feeding Platform (P3): Linear stepper motor (LM3) carrying two J-clamps,
- Guidewire Following/Rotation Platform (P4): Linear stepper motor (LM4) carrying a rotary stepper motor (RM2) and a guidewire torque device docking station.

For each instrument, the feeding platforms (P1 and P3) serve as an axial drive clamp, positioned at a defined distance from the instrument's corresponding entry point. This prevents buckling of instruments during remote (robot-assisted) manipulation as depicted in Fig. 4 (a). An example of the catheter insertion motion sequence is illustrated in Fig. 4 (b).

To address the requirement of seamless switching between remote (robot-assisted) and manual operations, quick release add-ons for the catheter (spur gear with Luer taper) and guidewire (guidewire clip) were developed to introduce rotary motion and to facilitate quick and safe dock/release. The magnified views of Fig. 3 illustrate both add-ons. The supplemental video presents the introduction of the catheter and guidewire to the robot in more detail.

2) Stepper Motors & Clamps

The pneumatic stepper motors used herein are adaptations of the motors designed, illustrated and discussed in [21], [22]. The linear motor (miniaturized variant of T-63) consists of two sealed, dual-acting pistons acting on a rack. The pistons and rack have a teeth pitch of $1.2\,\mathrm{mm}$ and a teeth depth of $2\,\mathrm{mm}$ resulting in a step size of $s_\mathrm{t} = 1.2/4 = 0.3\,\mathrm{mm}$. The motor measures $(32 \times 30 \times 16)\,\mathrm{mm}^3$ excluding the rack. The rotary motor (miniaturized version of R-80) consists of two sealed, dual-acting pistons placed in a cross configuration acting on a geared axle. The geared axle has 9 teeth with a circular pitch of 40° resulting in a step angle of $s_\mathrm{a} = 360^\circ/(9 \times 4) = 10^\circ$. The motor measures $(25 \times 25 \times 20)\,\mathrm{mm}^3$.The pneumatic J-clamp is a miniaturised, 3D printed double-acting cylinder. The clamp comprises two sealed chambers acting on a J-shaped piston with a protruding rod. Depending on which chamber is pressurised, the piston outstrokes or instrokes, with a stroke of $3.8\,\mathrm{mm}$. The clamp measures $(31 \times 25 \times 19)\,\mathrm{mm}^3$ excluding the piston. The theoretical force exerted by the piston is $F = P \cdot A = 79 \times 10^{-6} P$ (equivalent to $7.9\,\mathrm{N}$ at 1 bar).

3) Pneumatic Control

The robot is controlled by a pneumatic valve manifold, where each stepper motor (linear and rotary) is independently operated by a pair of 5/2-way directional control valves MHA2-MS1H-5/2-2 (FESTO AG and Co. KG, Esslingen, Germany). In the case of clamps, one valve controls a pair of clamps. In total, 14 valves are composed and driven by customised driver boards that interface digital outputs of employed real-time hardware (see Sec. IV). An oil free air compressor, Bambi PT15 (Air supplies, Nottingham, United Kingdom) is used to deliver pressurised air to the valves.

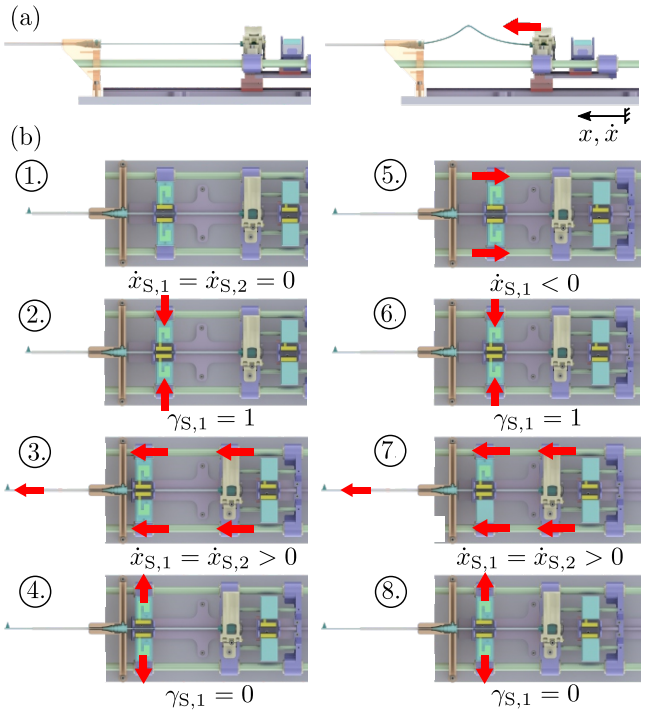

Fig. 4: (a) Illustration of catheter buckling during feeding due to unsupported length in free space. (b) Example of the insertion sequence. (1) Starting from the initial static position, (2) P1 clamps the catheter. (3) P1 and P2 move at the same speed (to avoid buckling) and for the same predefined entire stroke. (4) P1 releases the catheter and returns to the initial position, (5) while P2 stays still. (6) P1 clamps the catheter again. (7) P1 and P2 advance simultaneously half of the defined stroke. (8) P1 releases the catheter.

4) Robot Kinematics

For control purposes, the slave robot can be decomposed to two coupled robotic manipulators described by joint state $\boldsymbol{q}_{\mathrm{S},j}$ with $j = \{1, 2\}$. More explicitly, the state of the catheter driver is given by $\boldsymbol{q}_{\mathrm{S},1} = (x_{\mathrm{S},1}, x_{\mathrm{S},2}, \theta_{\mathrm{S},1})^{\mathrm{T}} \in \mathbb{R}^3$ and of the guidewire driver by $\boldsymbol{q}_{\mathrm{S},2} = (x_{\mathrm{S},3}, x_{\mathrm{S},4}, \theta_{\mathrm{S},2})^{\mathrm{T}} \in \mathbb{R}^3$. Clamping is described with binary vector $\boldsymbol{q}_{\mathrm{CL}} = (\gamma_{\mathrm{S},1}, \gamma_{\mathrm{S},2})^{\mathrm{T}}$. Kinematic parameters are described in detail in Fig. 3 and the composed joint state of the slave robot yields to

$$\boldsymbol{q}_{\mathrm{S}} = \left(\boldsymbol{q}_{\mathrm{S},1}, \boldsymbol{q}_{\mathrm{S},2}\right)^{\mathrm{T}} \in \mathbb{R}^6. \tag{2}$$

The proposed robotic system is capable of rotating both instruments infinitely in both directions, but this does not apply to translation. The executable insertion and retraction strokes are dependent on the states of each instrument. During insertion, the achievable strokes are:

$$s_{\mathrm{cat,ins}} = l_{\mathrm{rack}} - (x_{\mathrm{s},2} + b_1). \tag{3}$$
$$s_{\mathrm{gw,ins}} = x_{\mathrm{s},2} - (x_{\mathrm{s},4} + b_2); \tag{4}$$

where $s_{\mathrm{cat,ins}}$ and $s_{\mathrm{gw,ins}}$ are the executable insertion strokes of the catheter and guidewire respectively. b_1 is the width of platforms P1 and P4, b_2 is the width of platform P2, l_{rack} is the total length of the rack as shown in Fig. 3. For retraction:

$$s_{\mathrm{cat,ret}} = x_{\mathrm{s},2} - (b_2 + x_{\mathrm{s},4}). \tag{5}$$
$$s_{\mathrm{gw,ret}} = x_{\mathrm{s},4} - b_1; \tag{6}$$

where $s_{\mathrm{cat,ret}}$ and $s_{\mathrm{gw,ret}}$ are the achievable retraction strokes

of the catheter and guidewire respectively. Boundary conditions of positions $x_{s,2}$ and $x_{s,4}$ are:

$$(b_1 + b_2) < x_{\mathrm{s},2} < l_{\mathrm{rack}} - b_1; \quad (7)$$

$$b_1 < x_{\mathrm{s},4} < (b_1 + b_2). \quad (8)$$

5) Fabrication

The parts of the slave robot were printed with Objet 500 Connex3 (Stratasys Ltd., Eden Prairie, MN, USA) in materials VeroClear and VeroBlack (standard quality, glossy finish). The seals were laser-cut from $0.5\,\mathrm{mm}$ silicone rubber (Silex Ltd, Bordon, UK). The moving parts were lubricated and the motor/clamp housings and covers were glued together. Polyetheretherketone (PEEK) fasteners were used to assemble components and pairs of epoxy glass rods ($\varnothing\,10\,\mathrm{mm}$) and PEEK rods ($\varnothing\,6\,\mathrm{mm}$) were used to guide the platforms (Misumi Europa GmbH, Frankfurt, Germany).

6) MRI-Compatibility

Since the robot is composed of materials that are electrically non-conductive, non-metallic, and non-magnetic, it complies with the MR-Safe classification of the American Society for Testing and Materials (ASTM) standard F2503. A preliminary MR study was conducted as presented in Sec. V-C.

IV. CONTROL ARCHITECTURE

The system control architecture is based on the integration of the robotic system in Sec. III with subsequently described navigation system, which includes real-time image-guidance and haptic feedback. This configuration provides the following benefits: (1) the surgeon is always in control of the procedure, by teleoperating the slave robot through the master manipulator; (2) real-time navigation and haptic feedback guides the surgeon throughout the procedure increasing the instrument manipulation accuracy and minimising endothelial damages to the vessel wall, thus potentially improving the overall safety of the procedure.

The control architecture employs a host-target structure based on a PC (host), and two real-time controllers with FPGA (targets). The PC (Windows 7, Intel i7-6700, $3.4\,\mathrm{GHz}$, $16\,\mathrm{GB}$ RAM) runs the navigation system GUI ($30\,\mathrm{Hz}$), while the two real-time controllers (compactRIO 9022, National Instruments, Austin, TX, USA) run the control algorithms ($1\,\mathrm{kHz}$) for the haptic master device (1st target) and the slave robot (2nd target). The host PC and the targets communicate via Ethernet. User inputs are captured by the master manipulator, and processed by the control algorithms to generate corresponding motion commands on the slave robot which replicates the input into the surgical field. The overall system architecture is summarised in Fig. 5 (a) and further described below.

A. Navigation System

The navigation system, introduced in [18], has two main functions: (1) receive and display in real-time the intra-operative video of the surgical scene on a GUI; and (2) generate dynamic active constraints with safety margins (adaptively enforced in real-time to constrain the catheter motion) for vision-based haptic feedback. A real-time video stream of the surgical scene is acquired using an image grabber (DVI2USB3, Epiphan Video, Ottawa, Canada) from a vascular imaging system - in this study we used a fluoroscopic system for interventional radiology procedure (Innova 4100 IQ, GE Healthcare, Chicago, Il, USA). The video stream is displayed on the navigation system GUI and processed to generate vision-based haptic feedback. The matching pattern algorithm (NI Vision 2018, National Instruments, Austin, TX, USA) introduced in [18], was improved to track both catheter and guidewire in a fluoroscopy video stream providing tip position (in pixels) and orientation (in degrees). The vessel wall is dynamically tracked using the vessel tracker algorithm described in [18]. Data from instrument and vessel trackers are used to generate and render vision-based haptic feedback to the master device. The clinical user perceives a viscous friction which increases proportionally to the instrument-vessel distance (i.e. the closer the instrument is to the vessel, the higher is the generated force feedback). The viscous friction is modelled for both DOF as:

$$\dot{x}_{\mathrm{M}} = \frac{1}{\kappa_{\mathrm{d}}\kappa_{\nu}} I_{\mathrm{M,t}} \quad (9) \qquad \dot{\theta}_{\mathrm{M}} = \frac{1}{\kappa_{\mathrm{d}}\kappa_{\nu}} I_{\mathrm{M,a}}, \quad (10)$$

where $I_{\mathrm{M,t}}$ and $I_{\mathrm{M,a}}$ are surgeon inputs, i.e., currents of the linear and rotary motor when a force is applied on the user handle, $\dot{x}_{\mathrm{M}}$ and $\dot{\theta}_{\mathrm{M}}$ are control outputs (i.e. nominal master motor velocity), and $\kappa_{\mathrm{d}}\kappa_{\nu} > 0$ is the damping of the virtual contacts, i.e. κ_{d} is generated by the proximity of the catheter tip to the vessel wall, and κ_{ν} by the direction and orientation of motion of the catheter with respect to the vessel wall. A comprehensive description is provided in [18] and summarised as follows: (1) The viscous friction is minimum if the instrument is located in the centre of the vessel and not pointing toward the vessel wall, (2) The viscous friction increases if the instrument-wall distance is closer and moving toward the vessel wall.

B. Robot Control

Master velocities related to user input and navigation in Eq. (9) and Eq. (10) are mapped to the slave robot with

$$\dot{\boldsymbol{q}}_{\mathrm{S},j} = \begin{pmatrix} \dot{x}_{\mathrm{S},2j-1} \\ \dot{x}_{\mathrm{S},2j} \\ \dot{\theta}_{\mathrm{R},j} \end{pmatrix} = \underbrace{\begin{pmatrix} 1 & 0 \\ 1 & 0 \\ 0 & 1 \end{pmatrix}}_{\boldsymbol{B}} \underbrace{\begin{pmatrix} S_{\mathrm{t}} & 0 \\ 0 & S_{\mathrm{r}} \end{pmatrix}}_{\boldsymbol{S}} \begin{pmatrix} \dot{x}_{\mathrm{M}} \\ \dot{\theta}_{\mathrm{M}} \end{pmatrix}, \quad (11)$$

where matrix $\boldsymbol{S} \in \mathbb{R}^{2\times 2}$ applies input scaling for translation and rotation with user-adaptive scalars $S_{\mathrm{t}} \in \mathbb{R}_{>0}$ and $S_{\mathrm{r}} \in \mathbb{R}_{>0}$, $\boldsymbol{B} \in \mathbb{R}^{3\times 2}$ describes a selection matrix to sync both linear motors during feeding and retraction, and $j = \{1, 2\}$. According to the user selection, velocities are computed for actuators driving the catheter ($j = 1$) or guidewire manipulator ($j = 2$). Hence, nominal frequencies of pulse-width modulated (PWM) signal pairs for dual-valve control (see Sec. III-B) of each linear motor i yield to $f_{\mathrm{S},i} = \dot{x}_{\mathrm{S},i}/s_{\mathrm{t}}$ with $i = \{1, \ldots, 4\}$ and for each rotary motor to $f_{\mathrm{S},k} = \dot{\theta}_{\mathrm{S},k}/s_{\mathrm{a}}$ with $k = \{1, 2\}$. Phase shift $\phi = 0.25$ within signal pairs and duty cycle $\eta = 0.5$ are constant parameters of the corresponding period [21]. The maximum frequency for safe operating conditions of actuators is set to $f_{\max} = 35\,\mathrm{Hz}$

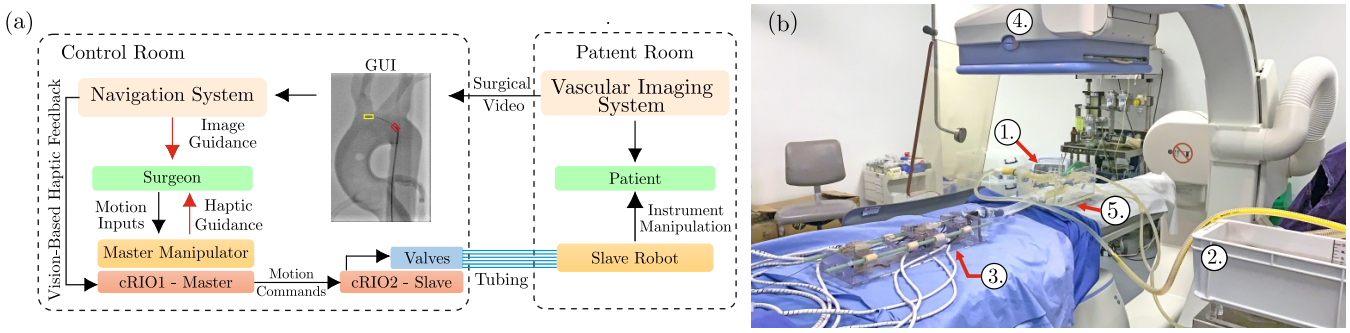

Fig. 5: (a) Control architecture and (b) experimental set-up for fluoroscopy-based trials, where (1) Vascular phantom, (2) Pulsatile and continuous flow pump, (3) Slave robot, (4) C-arm, (5) Force/Torque sensor

which allows linear actuator velocities of $\dot{x}_{\max} \approx 10\,\mathrm{mm\,s^{-1}}$ and angular velocities of $\dot{\theta}_{\max} \approx 300\,^{\circ}\,\mathrm{s^{-1}}$. The 12-channel PWM output is implemented on FPGA level for reliable timing.

V. Experimental Validation

A. Clinical Workflow and Set-Up for Robotics Procedure

The main system architecture is shown in Fig. 5 (a). The master device is placed in the control room of the CathLab together with the host PC running the navigation system. The latter is connected to the vascular imaging system to grab the surgical video, display it on the navigation GUI, and perform image processing as described in Sec. IV. Pneumatic valves, real-time controllers and air compressor are placed in the control room as well. Plastic tubes to connect valves and slave robot are passed through the wall between the control and patient rooms. The robotic slave is located on the surgical table in the patient room as depicted in Fig. 5 (a) close to the patient. This configuration presents two major benefits: (1) it allows the surgeon to perform the procedure from the control room, thus not being exposed to radiation when x-ray guidance is used; (2) it allows to perform an MRI-guided procedure by locating the entire hardware in the control room except of the MR-safe slave robot. When the robotic set-up is completed, the surgeon enters the patient room and manually accesses the arterial system as in a conventional procedure (e.g. through the femoral artery). Once, vascular access is gained, the instruments (catheter and guidewire) are connected to the slave robot, and the surgeon performs the surgical procedure using the master device from the control room. If needed, the procedure can be reverted to manual in a few seconds, by quickly releasing the instruments from the slave, as shown in the supplemental video.

B. X-Ray Fluoroscopy Pre-Clinical Trials

This section discusses the experimental set-up and methods undertaken to validate the robot in a number of simulated clinical scenarios, which involved a series of arterial cannulation maneuvers performed by a qualified vascular surgeon, both with the robot (i.e. using the clinical workflow above) and manually (i.e. using conventional techniques without the robot) under fluoroscopy guidance. Experiments were conducted in a research angiography theatre (Northwick Park Hospital, London, UK). The experimental set-up was as shown in Fig. 5 (b). A vascular phantom, a semi-radiolucent soft silicone full-scale model of a normal adult human aortic arch (Elastrat, Geneva, Switzerland), was rigidly coupled to 6-DOF force-torque sensor (Mini40, ATI Industrial Automation, Apex, NC, USA) to measure forces (25 Hz) applied to the vascular model during the procedure. This apparatus was placed underneath an x-ray imaging system (Innova 4100 IQ, GE Healthcare, Barrington, IL, USA) to simulate a patient lying on the angiography table to undergo an endovascular procedure. The robot was then positioned and oriented relative to the phantom to simulate access into the arterial system via the femoral artery. The phantom was connected to a pulsatile pump to simulate normal human blood flow. To reduce the effect of a learning curve, the operator was given a familiarization period of 6 min to manipulate the guidewire and catheter within the setup both manually and with the robot. A single guidewire (Radifocus Guide Wire M .035" 180 cm angled, Terumo, Tokyo, Japan) and catheter (Beacon Tip 5 Fr VanSchie2, Cook Medical, Bloomington, IN, USA) were used throughout the experiment. The operator was then asked to perform, in turn, by manipulation of wire and catheter, cannulation of 3 arteries with increasing difficulty in the following order: the left subclavian (LSA), left common carotid (LCCA) and right common carotid (RCCA) arteries. Each task consisted of traversing the descending aorta, navigating the aortic arch, and finally cannulating the artery. At the start of the experiment a coin toss was used to determine whether the first maneuver would be robotic or manual.

The operator performed cannulation of the nominated artery 4 times with the determined modality (i.e. robot or manual); each time, guidewire and catheter were returned to a standard starting position in the descending aorta. The task is repeated with the second modality. Attention was then turned to the next artery, and the above sequence was repeated. Modality was not changed upon moving to a new artery, so that at least one artery would be cannulated with the robot first, and at least one would be cannulated manually first. During each maneuver, fluoroscopy was activated by the operator using a pedal. The feed from the video display of the imaging system, the time taken for the maneuver, and fluoroscopy time were recorded. Within each sequence of 4 arterial cannulations, the first maneuver was excluded from the analysis, to minimize the effect of a learning curve. For each artery-modality pair, means and standard deviations

	LSA		LCCA		RCCA	
	Manual	Robotic	Manual	Robotic	Manual	Robotic
Mean force (N)	**0.37 ± 0.21**	**0.18 ± 0.09**	**0.59 ± 0.22**	**0.28 ± 0.12**	**0.68 ± 0.33**	**0.35 ± 0.18**
Maximum force (N)	1.01 ± 0.41	0.37 ± 0.04	**1.45 ± 0.09**	**0.68 ± 0.22**	1.85 ± 0.89	1.10 ± 0.29
Cannulation time (s)	**6.7 ± 4.5**	**50.0 ± 28.3**	**32.0 ± 2.8**	**65.0 ± 10.8**	58.3 ± 24.9	43.7 ± 15.0
Fluoroscopy time (s)	**9.7 ± 7.3**	**134.0 ± 48.6**	**69.3 ± 31.6**	**302.0 ± 56.0**	**86.7 ± 31.4**	**189.3 ± 9.0**

TABLE I: Results of fluoroscopy pre-clinical trials (mean ± SD). Bold values indicate statistically significant results ($p<0.05$) according to Student's t-test

were compared for: time taken for cannulation, fluoroscopy time, mean overall force, and mean maximum force. Results are summarised in Tab. I and discussed in Sec. VI.

C. MRI Preliminary Study

To demonstrate the versatility and MRI compatibility of the slave robot, a preliminary study was conducted in an MRI scanner. The robot was placed in an Achieva (3 T) MR imaging system (Philips Healthcare, Best, the Netherlands) equipped with a SENSE-Torso coil with 16 elements and placed adjacent to a plastic phantom of abdominal aorta filled with water (Elastrat Sàrl, Geneva, Switzerland). The phantom was placed inside the coil at the isocenter of the scanner as shown in Fig. 6 (a). With this setup, an MR-conditional guidewire (EPflex GmbH, Dettingen, Germany) was initially manipulated manually and then robotically. The guidewire consists of passive negative paramagnetic MR markers at discrete steps of 5 cm, which provide MRI visibility. The images were acquired using a 2D imaging sequence with a large slice thickness to project the guidewire and anatomy onto a plane, emulating a fluoroscopic projection. The 2D imaging sequence used was a real time 2D Turbo Spin Echo (TSE) with the shortest possible echo spacing. The MRI acquisition settings were:

- Echo Time (TE): 35 ms
- Repetition Time (TR): 536 ms
- Field of View (FOV): $(300 \times 142)\,\mathrm{mm}^2$
- Slice thickness: 100 mm
- Slice Orientation: coronal
- Dynamic scans: 100
- Total scan duration: 55.2 s

VI. Discussion

A. Fluoroscopy Pre-clinical Trials Results

Results reported in Tab. I show a reduction of forces applied to the phantom when the robotic system is used, compared with a conventional manual technique. Using the robot, the mean overall force exerted on the phantom is significantly (Students t-test) reduced by about 20% when cannulating LSA, and by more than 30% for LCCA and RRCA. This is corroborated by the analysis of maximum forces, which resulted in a reduction of up to 77% when LCCA is cannulated robotically. This may be related to the vision-based control architecture that automatically slows down the velocity of the robot when the instrument approaches the vessel wall (see Sec. IV).

From the clinical point of view, this is an important consideration, as dangerous collisions between instruments and vessel wall are minimised, thus increasing the overall safety of the procedure. On the other hand, this has the effect of increasing the procedure time when compared to manually performing the procedure, as reflected by the measured fluoroscopy times. This was expected, as the trials were conducted by a trained surgeon with relevant experience in manual catheterization but no formal training with the robotic platform. Therefore, a direct comparison of manual vs robotic procedures on this metric may not be fair at this stage. However, the results show that the robotic procedure mean fluoroscopy times were between 2 and 5 minutes. We believe that these times are acceptable and that this is a promising result, especially considering that the surgeon can operate the robot from outside the angiography room and therefore not exposed to radiation. Also, it is worth noting that the fluoroscopy time refers to the entire procedure, including the traversal of the descending thoracic aorta, the navigation of the aortic arch, and finally the cannulation of the target artery (LSA, LCCA, RCCA).

When comparing fluoroscopy with cannulation time (i.e. the time spent to cannulate only the target artery), it appears that when the robot is used, a high proportion of the time is spent navigating the descending aorta and the aortic arch. These relatively simpler tasks can be done more quickly manually. However, when a more complex task such as cannulation of the RCCA was performed, the robotic procedure time was comparable with (slightly shorter than) the manual. This suggests that the robot can be potentially employed in complex phases of the procedure (when manipulation accuracy and safety are more relevant than time), while manual manipulation can continue to be used for less critical phases that can be accomplished equally well and more quickly in this way. The proposed system lends itself to this approach, given its capability of quickly switching between robotic and manual manipulation. Overall, these trials demonstrated that robotic cannulation of the LSA, LCCA, and RCCA is feasible using the proposed platform. Surgeons skills are successfully captured by the master device and mapped to the slave robot to accomplish the cannulation.

B. MRI

Fig. 6 (b) and (c) show the projected MRI image of the manual and robotic retractions of the guidewire, with no geometric distortions detected during the robot manipulation. Fig. 6 (d) show the image difference between Figs. 6 (b) and (c). The bright spots in the subtraction image might be caused by collisions of the guidewire with the anatomy and susceptibility artifacts of the passive negative MR markers. The average signal intensity of the brightest patch and the standard deviation of the background (noise) were evaluated

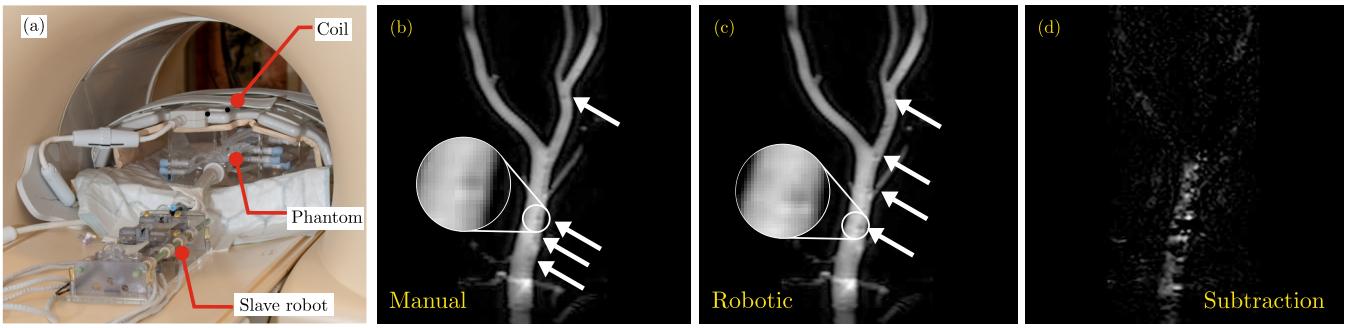

Fig. 6: (a) Experimental MRI set-up. Projection of abdominal aorta and iliac arteries with (b) manual and (c) robotic guidewire retraction. Magnified views show the passive MR markers of the guidewire (black spots), (d) Difference image.

for each image. The computed signal-to-noise ratio (SNR) show no significant change for both interventions (≈26 dB). The image sequences are presented in the supplemental video.

VII. Conclusions and Future Work

A master-slave system platform and a navigation framework for manipulation of standard endovascular instruments in different imaging environments has been developed. The proposed system was evaluated pre-clinically by cannulating three target arteries (LSA, LCCA and RCCA) under fluoroscopy guidance. Results show a reduction of forces applied when the robotic system is used compared to manual interventions. This was followed by a preliminary MRI compatibility experiment. The system shows its capability of manipulating instruments under MRI which not only potentially eliminates x-ray exposure, but also highlight its potential to improve manual MRI-guided treatment. In fact, based on [23], performing manual interventions under MRI creates additional challenges such as risk of musculoskeletal injury, which can, in turn, increase the possibility of medical errors and risk for the patient. Furthermore, this system paves the way to paediatric MRI-guided endovascular interventions. In future, the dynamics and latency of the master-slave system will be evaluated, different feeding and rotation mechanisms will be explored. Finally, a pre-clinical MRI study will be performed.

Acknowledgment

We would like to thank the King's College London MRI educational facilities staff: Dr. Ramesh Valapil, Mrs. Inka-Mari Granlund, Dr. Felipe Godinez; EPflex Feinwerktechnik GmbH, Dettingen, Germany for guidewire samples; Ying Xu for help with experiments and Jiwoo Choi for the photos.

References

[1] J. Kaplan, *Kaplan's Cardiac Anesthesia*, 7th ed. Elsevier, 2017.

[2] G.-Z. Yang *et al.*, "Medical robotics—regulatory, ethical, and legal considerations for increasing levels of autonomy," *Science Robotics*, vol. 2, no. 4, 2017.

[3] W. Saliba *et al.*, "Novel robotic catheter remote control system: feasibility and safety of transseptal puncture and endocardial catheter navigation," *J. Cardiovasc. Electrophysiol.*, vol. 17, no. 10, pp. 1102–1105, Oct 2006.

[4] E. M. Khan *et al.*, "First experience with a novel robotic remote catheter system: Amigo™ mapping trial," *Journal of Interventional Cardiac Electrophysiology*, vol. 37, no. 2, pp. 121–129, Aug 2013.

[5] J. Bismuth *et al.*, "A first-in-man study of the role of flexible robotics in overcoming navigation challenges in the iliofemoral arteries," *Journal of Vascular Surgery*, vol. 57, no. 2, Supplement, pp. 14S – 19S, 2013.

[6] J. F. Granada *et al.*, "First-in-human evaluation of a novel robotic-assisted coronary angioplasty system," *JACC: Cardiovascular Interventions*, vol. 4, no. 4, pp. 460 – 465, 2011.

[7] Y. Thakur *et al.*, "Design and performance evaluation of a remote catheter navigation system," *IEEE Transactions on Biomedical Engineering*, vol. 56, no. 7, pp. 1901–1908, July 2009.

[8] Y. Song *et al.*, "Haptic feedback in robot-assisted endovascular catheterization," *2017 IEEE International Conference on Mechatronics and Automation, ICMA 2017*, pp. 404–409, 2017.

[9] G. Bian *et al.*, "An enhanced dual-finger robotic Hand for Catheter manipulating in vascular intervention: A preliminary study," *2013 IEEE International Conference on Information and Automation, ICIA 2013*, pp. 356–361, 2013.

[10] S. Guo *et al.*, "High precise haptic device for the robotic catheter navigation system," in *2016 IEEE International Conference on Mechatronics and Automation, IEEE ICMA 2016*, 2016.

[11] K. Wang *et al.*, "Design and Performance Evaluation of Real-time Endovascular Interventional Surgical Robotic System with High Accuracy," *The International Journal of Medical Robotics and Computer Assisted Surgery*, vol. 14, no. 5, 2018.

[12] M. A. Tavallaei *et al.*, "A magnetic-resonance-imaging-compatible remote catheter navigation system," *IEEE Transactions on Biomedical Engineering*, vol. 60, no. 4, pp. 899–905, April 2013.

[13] K. Lee *et al.*, "Mr safe robotic manipulator for mri-guided intracardiac catheterization," *IEEE/ASME Transactions on Mechatronics*, vol. 23, no. 2, pp. 586–595, April 2018.

[14] H. Rafii-Tari *et al.*, "Current and emerging robot-assisted endovascular catheterization technologies: A review," *Annals of Biomedical Engineering*, vol. 42, no. 4, pp. 697–715, Apr 2014.

[15] L. Muller *et al.*, "Remote control catheter navigation: options for guidance under mri," *Journal of Cardiovascular Magnetic Resonance*, vol. 14, no. 1, p. 33, Jun 2012.

[16] N. Whiting *et al.*, "Real-time mri-guided catheter tracking using hyperpolarized silicon particles," *Scientific Reports*, vol. 5, Aug 2015.

[17] C. J. Payne *et al.*, "A force feedback system for endovascular catheterisation," in *2012 IEEE/RSJ International Conference on Intelligent Robots and Systems*, Oct 2012, pp. 1298–1304.

[18] G. Dagnino *et al.*, "Haptic feedback and dynamic active constraints for robot-assisted endovascular catheterization," in *2018 IEEE/RSJ International Conference on Intelligent Robots and Systems (IROS)*, Oct 2018, pp. 1770–1775.

[19] H. Rafii-Tari *et al.*, "Objective assessment of endovascular navigation skills with force sensing," *Annals of Biomedical Engineering*, vol. 45, no. 5, pp. 1315–1327, May 2017.

[20] W. S. Moore, "Arterial access; guidewires, catheters, and sheaths; and balloon angioplasty catheters," in *Vascular and Endovascular Surgery: A Comprehensive Review*. Saunders, 2013, ch. 17, pp. 306–309.

[21] V. Groenhuis and S. Stramigioli, "Rapid prototyping high-performance mr safe pneumatic stepper motors," *IEEE/ASME Transactions on Mechatronics*, vol. 23, no. 4, pp. 1843–1853, Aug 2018.

[22] V. Groenhuis *et al.*, "Dual-speed mr safe pneumatic stepper motors," in *Robotics: Science and Systems 2018*, June 2018.

[23] F. Fernndez Gutirrez *et al.*, "Comparative ergonomic workflow and user experience analysis of mri versus fluoroscopy-guided vascular interventions: an iliac angioplasty exemplar case study," *International journal of computer assisted radiology and surgery*, vol. 10, pp. 1639–1650, 10 2015.